

## Analysis of Thermal Stresses around a Cryosurgical Probe

YOED RABIN\*·† AND PAUL S. STEIF\*

\*Department of Mechanical Engineering, Carnegie Mellon University, 5000 Forbes Avenue, Pittsburgh, Pennsylvania 15213-3890; and †Division of Surgical Oncology, Allegheny General Hospital, Pittsburgh, Pennsylvania 15212

Large thermal stresses easily exceeding the tissue yield strength may develop in the frozen region around a cryosurgical probe. A new integrodifferential solution for the heat transfer problem of biological tissues freezing around a cryosurgical probe is presented in this article. This solution is suitable for cases of high Stephan numbers and for a temperature-dependent forcing function at the cryoprobe. A new solution for the thermal stresses around a cryosurgical probe is also presented, based on an elastic–perfectly plastic model. It is proposed that thermal stresses beyond the elastic limit of the frozen region may sharply increase the mechanical damage to the cell membranes due to plastic deformation. It was found that plastic deformation always starts at the cryoprobe surface; however, plastic deformation may also be formed near the freezing front at high cooling rates and large cryoprobes. It is demonstrated that under some conditions plastic deformation may occur in the entire frozen region. A parametric study to identify the best cooling protocol for maximal plastic deformation is presented. © 1996 Academic Press, Inc.

Cryosurgical success, or maximal destruction of undesired biological tissue by freezing, is influenced by many factors: the cooling rate (11, 14, 33), the thawing rate (25), the minimal temperature achieved (13), and repeated freezing–thawing cycles (14, 30). The mechanisms of destruction may generally be separated into two groups; the first is related to the freezing process within the phase transition temperature range, while the second group is related to further destruction after phase transition has been completed. Destruction mechanisms of the first group are related to heat transfer, mass transfer, and chemical equilibrium in the intracellular and extracellular solutions (22–24). Mechanical interaction between ice crystals and cells also affect the destruction process during the phase transition process (19).

Destruction mechanisms after the phase transition has been completed may be related to thermal stresses in the frozen region, as suggested by Rubinsky *et al.* (31), and as reported elsewhere (11, 18). It was suggested that the deformation resulting from these stresses may cause mechanical damage to the

cell's membrane. High thermal stresses may develop due to large temperature differences at the frozen region, as is the case in a typical cryosurgical procedure. For a spherical cryoprobe and typical physical properties of ice, the thermal stresses under some conditions can reach the yield strength of the material. It is proposed in this study that thermal stresses beyond the yield strength of the frozen material may severely increase the mechanical damage to the cell's membrane due to plastic deformation.

The mathematical model employed in this article rests on four principal assumptions: (a) the temperature distribution can be determined independently of the deformation of the tissue; (b) all deformations are small; (c) the frozen tissue may be modeled as an elastic–perfectly plastic solid; and (d) the problem is one-dimensional in the radial direction of a spherical coordinate system.

Initial stresses are always formed immediately after freezing due to the volume expansion of water at the freezing process. The distribution of these initial stresses is difficult to predict because the volume expansion is dependent on the internal ice structure which in turn is affected by many factors. It is as-

---

Received August 15, 1995; accepted January 8, 1996.

sumed in this study that the initial stresses can be neglected in comparison with the high thermal stresses which develop later in the cryoprocure.

A new simplified mathematical solution for the temperature distribution in biological tissues freezing around a cryosurgical probe is presented in this article. This solution is an improvement of an earlier solution proposed by Cooper and Trezek (7) in that it is suitable for high Stephan numbers and allows for a temperature-dependent forcing function at the cryoprobe. The differences between the earlier and the new solutions were found to be very significant in the short term, when the thermal stresses may be as high as the yield strength. Further, a new solution of the thermal stress problem around cryosurgical probe is presented, which makes use of the temperature solution.

HEAT TRANSFER ANALYSIS

A solution of the freezing process in biological tissue around a spherical cryoprobe is presented here under the following assumptions: (a) the thermal conductivity and the specific heat are constant thermophysical properties, possessing different values above and below the freezing temperature; (b) blood perfusion is constant in time and uniformly distributed in space in the unfrozen region; and (c) the metabolic heat generation effect can be neglected with respect to blood perfusion and the thermal interference of the cryoprobe.

The ‘‘classical’’ bioheat equation is assumed to be the governing equation of the heat transfer process (27):

$$\frac{k_l}{r^2} \frac{\partial}{\partial r} \left( r^2 \frac{\partial T_l}{\partial r} \right) + \dot{w}_b C_b (T_b - T_l) = C_l \frac{\partial T_l}{\partial t}$$

$$T_l > T_m. \quad [1]$$

Since the first presentation of the above bioheat equation, tremendous developments in modeling the effect of blood flow on heat transfer in biological tissues have been suggested (6, 20, 35, 36). A summary and a discussion regarding those models are presented

by Charny (4) and Diller (8). Most of the new models deal with relatively high temperatures—normal body temperatures and higher, and not with temperatures near freezing, as is the case here. Furthermore, based on experimental data it has been demonstrated that the classical bioheat equation can be used for engineering calculations of heat transfer during cryosurgery (29). Therefore, the classical bioheat equation is assumed to be an adequate model given the relative simple thermal stress analysis present here.

It is further assumed that blood perfusion decays with freezing and therefore the governing equation reduces to an ordinary heat diffusion equation:

$$\frac{k_f}{r^2} \frac{\partial}{\partial r} \left( r^2 \frac{\partial T_f}{\partial r} \right) = C_f \frac{\partial T_f}{\partial t} \quad T_m > T_f. \quad [2]$$

The boundary condition at the freezing interface is

$$k_f \frac{\partial T_f}{\partial r} (S, t) = k_l \frac{\partial T_l}{\partial r} (S, t) + L \frac{dS}{dt} \quad [3]$$

and its initial condition is:

$$S(0) = 0. \quad [4]$$

The boundary and initial conditions of the unfrozen region are, respectively:

$$T_l(S, t) = T_m; \quad \frac{\partial T_l}{\partial r} (\infty, t) = 0 \quad [5]$$

$$T_l(r, 0) = T_0(r); \quad T_0(R) = T_m. \quad [6]$$

The boundary and initial conditions of the frozen region are, respectively:

$$T_f(R, t) = T_R(t); \quad T_f(S, t) = T_m \quad [7]$$

$$T_f(r \rightarrow R, t \rightarrow 0) = T_m, \quad [8]$$

where the initial temperature distribution  $T_0$  and the cryoprobe forcing function  $T_R$  are known arbitrary functions. For simplicity of the presentation, the solution will be given in terms of the following temperatures differences:

$$\theta_f = T_f - T_m; \quad \theta_l = T_l - T_b. \quad [9]$$

The exact solution of the problem defined by Eqs. [1]–[8] is not known; therefore, an approximate analytical solution is derived here. The solution is performed by the integral method (15), in which the temperature distribution in each region is assumed to satisfy all its boundary conditions, and where the constants of each assumed temperature distribution are found to satisfy the integral form of the heat balance equation. The integral form of the bioheat equation in the unfrozen and frozen regions are, respectively:

$$\int_S^\infty k_l \frac{\partial}{\partial r} \left( r^2 \frac{\partial \theta_l}{\partial r} \right) dr - \int_S^\infty \dot{w}_b C_b \theta_l r^2 dr = \int_S^\infty C_l \frac{\partial \theta_l}{\partial t} r^2 dr \quad [10]$$

$$\int_R^S k_f \frac{\partial}{\partial r} \left( r^2 \frac{\partial \theta_f}{\partial r} \right) dr = \int_R^S C_f \frac{\partial \theta_f}{\partial t} r^2 dr. \quad [11]$$

The left terms in Eqs. [10] and [11] can be integrated explicitly, and the equations can be rewritten in the forms:

$$k_l S^2 \frac{\partial \theta_l}{\partial r} (S, t) = -C_l \frac{\partial}{\partial t} \int_S^\infty \theta_l r^2 dr - \dot{w}_b C_b \int_S^\infty \theta_l r^2 dr \quad [12]$$

$$k_f S^2 \frac{\partial \theta_f}{\partial r} (S, t) = k_f R^2 \frac{\partial \theta_f}{\partial r} (R, t) + C_f \frac{\partial}{\partial t} \int_R^S \theta_f r^2 dr. \quad [13]$$

The inner boundary, Eq. [3], can be rewritten in terms of Eqs. [12]–[13] to yield:

$$\begin{aligned} \frac{\partial}{\partial t} \left[ C_f \int_R^S \theta_f r^2 dr + C_l \int_S^\infty \theta_l r^2 dr \right] \\ + k_f R^2 \frac{\partial \theta_f}{\partial r} (R, t) + \dot{w}_b C_b \int_S^\infty \theta_l r^2 dr \\ = LS^2 \frac{dS}{dt}. \quad [14] \end{aligned}$$

By assuming a quasi-steady process the

temperature distribution in the unfrozen region becomes:

$$\theta_l = (T_m - T_b) \frac{S}{r} \exp\left(\frac{S-r}{\gamma}\right); \quad \gamma = \sqrt{\frac{k_l}{\dot{w}_b C_b}} \quad [15]$$

and in the frozen region:

$$\theta_f = (T_R - T_m) \frac{R(S-r)}{r(S-R)}. \quad [16]$$

The temperature distributions in Eqs. [15]–[16] are exactly the temperature distributions at a steady-state condition, when the freezing front location,  $S$ , reaches its final distance from the cryoprobe. Equations [15]–[16] satisfy all boundary conditions as defined above, but are dependent on the freezing front location.

Finally, the integral form of the inner boundary condition, Eq. [14], is solved to yield the time-dependent interface location,  $S$ . Using the assumed temperature distributions,  $\theta_l$  and  $\theta_f$ , Eq. [14] is reduced to a first-order ordinary differential equation in time:

$$\begin{aligned} \frac{d}{dt} \left\{ \frac{S^3}{3} + \frac{St_f R}{6} [S(S+R) - 2R^2] \right. \\ \left. + St_l S \gamma (S + \gamma) \right\} = \frac{\alpha_f St_f SR}{(S-R)} \\ - \frac{\dot{w}_b C_b}{C_l} St_l S \gamma (S + \gamma) \quad [17] \end{aligned}$$

which can only be solved numerically.

#### THERMAL STRESSES ANALYSIS

All physical properties of the frozen tissue are assumed constant in time and uniformly distributed in space, and are independent of the temperature and the strain. The material is assumed to be described by the following constitutive law in axial tension:

$$\dot{\epsilon} = \dot{\epsilon}^E + \dot{\epsilon}^P + \dot{\epsilon}^T. \quad [18]$$

Under the assumption of isotropy, the elastic strain rate is given by:

$$\dot{\epsilon}^E = \frac{\dot{\sigma}}{E} \equiv \bar{\sigma} \quad [19]$$

and the plastic strain rate by:

$$\dot{\epsilon}^P = \begin{cases} -\frac{2}{3} \dot{\lambda} & \sigma = \sigma_y \text{ and } \dot{\sigma} = 0 \\ 0 & \sigma < \sigma_y \text{ or } \dot{\sigma} < 0. \end{cases} \quad [20]$$

The material is taken to be nonhardening (perfectly plastic) in which case  $\dot{\lambda}$  cannot be determined from the stress.

For spherical symmetry there are no shear stresses, the condition for mechanical equilibrium simplifies to:

$$\frac{d\bar{\sigma}_r}{dr} + \frac{2(\bar{\sigma}_r - \bar{\sigma}_\theta)}{r} = 0. \quad [21]$$

Note that the stresses are normalized by the elastic module,  $E$ . Finally, the strain-displacement relations are given by:

$$\epsilon_r = \frac{du_r}{dr}; \quad \epsilon_\theta = \frac{u_r}{r}. \quad [22]$$

A multiaxial stress generalization of Eq. [20] based in the Mises invariant (17) is employed in which case the yield condition is:

$$|\bar{\sigma}_\theta - \bar{\sigma}_r| = \frac{\sigma_y}{E} = \epsilon_y \equiv \bar{\sigma}_y. \quad [23]$$

One can avoid the incremental formulation (i.e., strain rates) when  $\sigma_\theta - \sigma_r$  varies monotonously (referred to as proportional loading in plastic theory); then the plastic strains are given by:

$$\epsilon_r^P = -\frac{2}{3} \lambda; \quad \epsilon_\theta^P = +\frac{1}{3} \lambda. \quad [24]$$

The elastic strains are then given by:

$$\epsilon_r^E = \bar{\sigma}_r - 2\nu\bar{\sigma}_\theta; \quad \epsilon_\theta^E = (1 - \nu)\bar{\sigma}_\theta - \nu\bar{\sigma}_r. \quad [25]$$

The thermal strains are given by:

$$\epsilon_r^T = \epsilon_\theta^T \equiv \epsilon^T = \beta(T - T_m). \quad [26]$$

Finally, it is assumed that the unfrozen tissue cannot support normal stresses and therefore:

$$\bar{\sigma}_r(S) = 0. \quad [27]$$

Since that the cryoprobe yield strength is at least two orders of magnitude higher than of ice and since the thermal expansion coefficient of metals is at least one order of magnitude smaller than of ice (2), it is assumed that the displacement at the cryoprobe surface can be neglected:

$$u_r(R) = 0. \quad [28]$$

The well-known solution for the fully elastic problem ( $|\sigma_\theta - \sigma_r| < \sigma_y$  everywhere) is derivable from the above equations in terms of the temperature distribution. The elastic solution ceases to be valid when  $|\sigma_\theta - \sigma_r|$  reaches  $\sigma_y$  at some point. This is found to occur at the cryoprobe surface; thus, there develops a plastic region around the cryoprobe  $R < r < P$ , while the rest of the frozen region remains elastic,  $P < r < S$ . The interface between the plastic and elastic regions,  $P$ , is defined here as the plastic front. The following additional plastic front conditions thereby arise:

$$\bar{\sigma}_r(P)|^- = \bar{\sigma}_r(P)|^+; \quad u_r(P)|^- = u_r(P)|^+ \quad [29]$$

$$|\bar{\sigma}_\theta(P) - \bar{\sigma}_r(P)| = \bar{\sigma}_y, \quad [30]$$

where the “-” and “+” signs denote limits as the plastic-elastic interface is approached from the plastic and elastic regions, respectively.

### Elastic Region

The solution of stresses in the elastic region after the formation of the plastic front will be addressed first. This period, which starts with the formation of the plastic front, is defined as stage II. The solution of the elastic region is derived from the above formulation and is similar to the general solution presented by Boley and Weiner (3). The general solution of the dimensionless thermal stresses in the radial and tangential directions is:

$$\bar{\sigma}_r = -\frac{2}{1-\nu} \frac{1}{r^3} \int_P^r \epsilon^T r^2 dr + \frac{B_2}{1-2\nu} - \frac{2B_1}{1+\nu} \frac{1}{r^3} \quad P < r < S \quad [31]$$

$$\bar{\sigma}_\theta = \frac{1}{1-\nu} \frac{1}{r^3} \int_P^r \epsilon^T r^2 dr + \frac{B_2}{1-2\nu} + \frac{B_1}{1+\nu} \frac{1}{r^3} - \frac{\epsilon^T}{1-\nu} \quad P < r < S \quad [32]$$

where  $B_1$  and  $B_2$  are integration constants that can be found from boundary conditions. The integration constant  $B_1$  is calculated by substituting Eqs. [31]–[32] into boundary condition (30), leading to:

$$B_1 = \frac{1}{3} (1 + \nu) P^3 \left[ \bar{\sigma}_y + \frac{\epsilon^T(P)}{1-\nu} \right]. \quad [33]$$

Boundary condition Eq. [27] then allows the second integration constant to be determined:

$$B_2 = \frac{2(1-2\nu)}{S^3} \left[ \frac{\beta(T_R - T_m)}{1-\nu} \times \frac{R(S^2 - 2P^2)(S - P)}{6(S - R)} + \frac{B_1}{1+\nu} \right]. \quad [34]$$

To provide some context to the reader, we cite again a previous study reported by Rubinsky *et al.* (31), which was motivated by cryopreservation. They also solved a spherically symmetric thermal stress problem; by contrast, however, the freezing front propagates from some fixed outer surface toward the origin, the tissue is modeled as linear elastic, Eqs. [31]–[32], and the temperature distribution is different. In particular, they obtained the temperature distribution by assuming that the Stephan number is relatively small and that there is no blood perfusion (conditions which are not typical of cryosurgery). Because the two problems are rather different, quantitative comparison of results appear not to be warranted.

### Plastic Region

Substitution of the plastic yield condition, Eq. [23], into Eq. [21] implies the following form for the radial stress in the plastic region:

$$\bar{\sigma}_r = 2\bar{\sigma}_y \ln(B_3 r), \quad [35]$$

where the integration constant  $B_3$  is calculated by forcing continuity in the radial stress at the plastic front, Eq. [29]:

$$B_3 = \frac{1}{P} \exp \left[ \frac{1}{2\bar{\sigma}_y} \left( \frac{B_2}{1-2\nu} - \frac{2B_1}{1+\nu} \frac{1}{P^3} \right) \right]. \quad [36]$$

The tangential stress is calculated directly from the plasticity condition, Eq. [23]:

$$\bar{\sigma}_\theta = \bar{\sigma}_y [1 + 2 \ln(B_3 r)]. \quad [37]$$

Introducing the strains, Eq. [24]–[26] into the strain–displacement relations, Eq. [22], yields:

$$\lambda = \beta(T_R - T_m) \frac{3}{2} \frac{R}{r} \frac{S}{(S - R)} - 3\bar{\sigma}_y(1 - \nu) + \frac{B_4}{r^3}. \quad [38]$$

Integration constant  $B_4$  is calculated by forcing continuity in displacement at the plastic front, Eq. [29]:

$$B_4 = -3R^3 \left[ 2\bar{\sigma}_y(1 - 2\nu) \ln(B_3 R) + \epsilon^T(R) + \frac{\beta S(T_R - T_m)}{2(S - R)} \right]. \quad [39]$$

The solution of the thermal stress problem is well defined now, as long as the plastic front location,  $P$ , is known. Unfortunately, an explicit expression for  $P$  is impossible to obtain and therefore a trial-and-error procedure is needed as follows: (a) estimating  $P$  in the range  $R$  to  $S$ ; (b) calculating  $B_1$ ,  $B_2$ ,  $B_3$ ,  $B_4$  by that order; and, (c) comparing the displacements on both sides of the plastic front, Eq. [29]. As a verification of the calculation  $\lambda(P)$  must equal 0.

### Initiation Stage

The initiation stage (also termed stage I) is defined as starting from the onset of freezing until first plastic yielding. The stresses at this stage will be the same as presented by Eqs. [31]–[32], with the only exception that the lower boundary for integration will be  $R$  instead of  $P$ . Boundary conditions of zero radial stress at the freezing front and zero displacement at the cryoprobe surface will yield:

$$B_1 = -\beta(T_R - T_m) \times \frac{2(1 - 2\nu)(1 + \nu)}{(2 - \nu)(1 - \nu)} \frac{R^4[S(S + R) - 2R^2]}{6S^3} \quad [40]$$

and

$$B_2 = -\frac{B_1}{R^3}. \quad [41]$$

### DISCUSSION

The heat transfer analysis is addressed first in this discussion. The proposed solution of the freezing process is an integrodifferential solution. It may be argued that the heat transfer problem could have been solved numerically for the more general case of temperature-dependent thermophysical properties and phase transition temperature range, by finite element (16, 21, 32) or finite difference techniques (28). Despite the above argument, there are three main reasons for developing the new freezing solution. First, an explicit expression of temperature distribution leads to an explicit expression for stress distribution, which would not be the case for numerical solution. This simplifies much the analysis of the thermal stress problem. Second, the approximate solution presented here can be performed much faster than a complete numerical solution. For example, a one-dimensional heat transfer problem demands the simultaneous solution of  $n$  equations at  $n$  grid points at each time interval, while the new proposed solution demands a solution of only Eq. [17], at each time. Finally, modeling of stresses in this

study relies on several simplifications, the most important one being that frozen biological tissues behave like an elastic–perfectly plastic solid. Thus, it seems that a more accurate solution for the heat transfer problem is not warranted.

The heat transfer solution may be further simplified by neglecting the heat capacity of the frozen and unfrozen regions with respect to the latent heat. In this case the transient terms of the heat balance Eqs. [1]–[2] can be neglected and the freezing front location will have an explicit form, as presented first by Cooper and Trezek (7) [C & T]. The condition holds when Stephan number is much less than unity. Unfortunately, for typical thermophysical properties of soft biological tissues, Table 1, and for cryogenic temperature differences, the Stephan number is 1 or even larger. Figure 1 presents a comparison of the freezing front location as calculated by C & T and by the new proposed solution. As can be seen from Fig. 1, the freezing front location of both solutions coincides in the long term as the frozen region reaches its final size. However, the differences between the two solutions are very significant in the short term. For example, the time needed for a frozen region of 10 mm in radius to form according to the present solution is about three times that calculated by C & T for a high blood perfusion rate (50 kW/m<sup>3</sup>·°C). The heat transfer solution and the computer code were validated by examining the case in which the specific heat of both the frozen and unfrozen regions are set to zero and all the other thermophysical properties remain the same as above. It was found in this test that the new proposed solution coincides with that of C & T at all times.

In contrast to the C & T solution, the new proposed solution enables an arbitrary temperature forcing function at the cryoprobe. With this solution, the temperature distributions in the frozen and unfrozen regions become more accurate as the cooling rate at the cryoprobe decreases. Figure 1 presents the freezing front location associated with a cooling rate of 50°C/min, which may be reasonable for a low-

TABLE 1  
Typical Thermophysical Properties of Biological Tissues and Ice (1, 5, 12)

	Soft tissues	Water
Freezing temperature, $T_m$ , °C	-3	0
Latent heat, $L$ , MJ/m <sup>3</sup>	250	331.7
Thermal conductivity in the unfrozen region, $k_i$ , W/m-°C	0.5	0.595 (15°C)
Thermal conductivity in the frozen region, $k_f$ , W/m-°C	2	2.25
Specific heat in the unfrozen region, $C_i$ , MJ/m <sup>3</sup> -°C	3.8	4.186 (15°C)
Specific heat in the frozen region, $C_f$ , MJ/m <sup>3</sup> -°C	1.9	1.133
Specific heat source of blood, $w_b C_b$ , kW/m <sup>3</sup> -°C	0-50	0
Metabolic heat generation, $q_{met}$ , kW/m <sup>3</sup>	0-22	0

powered cryoprobe. As will be presented shortly, the stresses formed at the beginning of the freezing process are relatively high and are significantly influenced by the cooling rate of the cryoprobe; this motivates the development of the new solution.

The thermal stresses analysis is addressed next. The dimensionless stresses,  $\sigma_r$  and  $\sigma_\theta$ , and the plastic front location,  $P$ , are strong

functions of the yield strain,  $\epsilon_y$  ( $=\sigma_y/E$ ). Although there is a large variation in the separate values for the yield strength and the elastic module (Table 2), the yield strain,  $\epsilon_y$ , for ice is expected to be in the range of  $0.5 \times 10^{-3}$  to  $1 \times 10^{-3}$ . However, this parametric study deals with the extreme cases as well, in the range 0 to  $5 \times 10^{-3}$ . Unless otherwise specified in this parametric study, the following

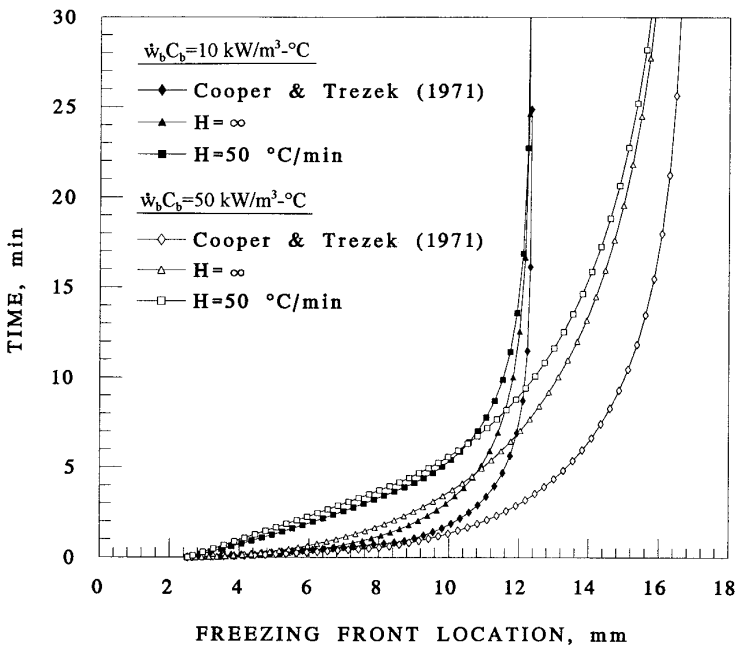


FIG. 1. Comparison of the time required for freezing front propagation, as calculated by Cooper and Trezek (7) and by the present solution. Typical thermophysical properties of soft biological tissues and cryoprobe diameter of 5 mm.

TABLE 2  
 Typical Physical Properties of Ice (9, 12, 26, 34)

Thermal expansion coefficient $\beta$ , $1/^\circ\text{C}$	$55 \times 10^{-6} (-4^\circ\text{C}) - 38 \times 10^{-6} (-80^\circ\text{C})$
Yield strength, $\sigma_y$ , MPA	0.4–13
Young's module, $E$ , GPa	0.3–10
Poisson's ratio, $\nu$	0.33

conditions were used: typical thermophysical properties of soft biological tissues, Table 1, specific heat source of the blood of  $\dot{w}_b C_b = 25 \text{ kW/m}^3\text{-}^\circ\text{C}$ , cooling rate of  $200^\circ\text{C}/\text{min}$  at the cryoprobe, and cryoprobe diameter of 5 mm. Since the relevant physical properties of frozen soft tissues are essentially unavailable, the mechanical properties of ice will be assumed when needed.

It simplifies the mathematical solution to assume that the thermal expansion coefficient,  $\beta$ , has a constant value throughout the entire range of cryogenic temperatures. However, the expansion coefficient,  $\beta$ , does decrease with temperature below the freezing temperature (12). For the purpose of the present parametric study, it might seem reasonable to take the mean value of this physical property over the cryogenic temperature range. However, since a spherical problem is considered here, in which most of the temperature profile is above the mean of the two extreme limits, it seems more accurate to calculate the average temperature based on an integral over the volume of the frozen region. This somewhat higher value for the average temperature was the basis for choosing the expansion coefficient of  $45 \times 10^{-6} 1/^\circ\text{C}$ , which was used in this study. It is noted that an underestimation of the thermal expansion coefficient will lead to an underestimation of the thermal stresses.

Two typical cases of stress formation are considered first. Cases A and B are for a relatively high and an expected value of the yield strain,  $5 \times 10^{-3}$  and  $5 \times 10^{-4}$ , respectively. The resulting thermal stresses for case A are presented by Fig. 2 at the end of stages I and II, which are the initiation stage and the stage after first plastic front formation, respectively. Stage II of case A ends close to a steady-state

condition when the frozen region diameter is about 95% of its final size. At the end of stage I it can be seen that both stress distributions reach their maximal value at the cryoprobe surface and that the tangential stress is about four times of the radial stress at the cryoprobe surface. The stress distributions become much different at the end of stage II. At this time the tangential stress reaches its maximal compressive value at the plastic front. The radial stress reaches its maximal value in the elastic region, at the radius in which the stresses in both direction have the same value. The tangential stresses are higher than the radial stresses in the plastic region. It is noted that the radial stress is 0 at the freezing front by definition while the tangential stress is compressive at this interface, and is very significant in magnitude.

The relationship between the freezing front and the plastic front locations is presented by Fig. 3. The plastic front location is almost a linear function of the freezing front location until some critical value and decays to a constant value as the heat transfer problem approaches a steady state. Figure 3 presents the effect of blood perfusion on the thermal stresses in case A. It can be seen that this relationship is completely independent of the blood perfusion in the steady state and is relatively insensitive in general, even in extreme cases of blood perfusion. It is noted that the diameter of the frozen region with a relatively low blood perfusion ( $5 \text{ kW/m}^3\text{-}^\circ\text{C}$ ) is about twice the diameter when blood perfusion is high ( $50 \text{ kW/m}^3\text{-}^\circ\text{C}$ ).

Very different stress distributions are observed in case B, as presented by Fig. 4. Stage II ends in case B as plastic deformation starts to form at the freezing front or, alternatively,

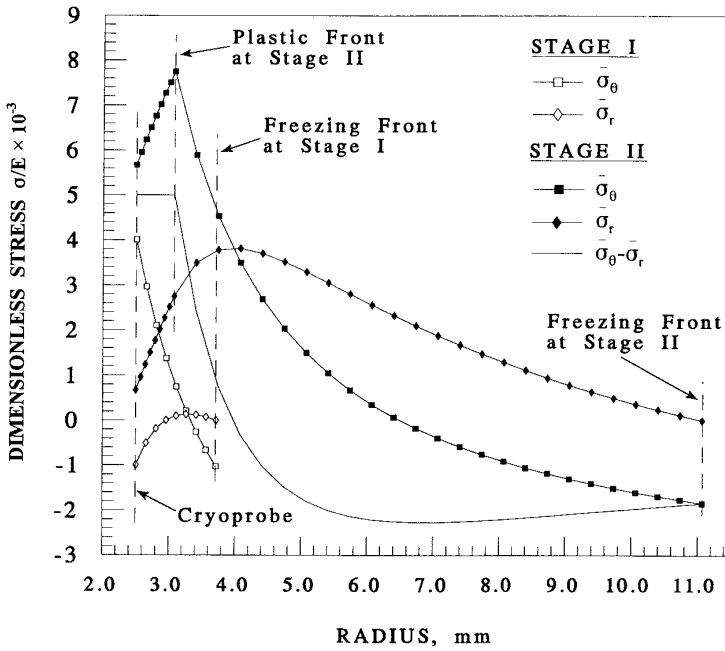


FIG. 2. Stress distributions around a spherical cryoprobe, for the case of relatively high yield strain,  $\epsilon_y = 5 \times 10^{-3}$  (case A).

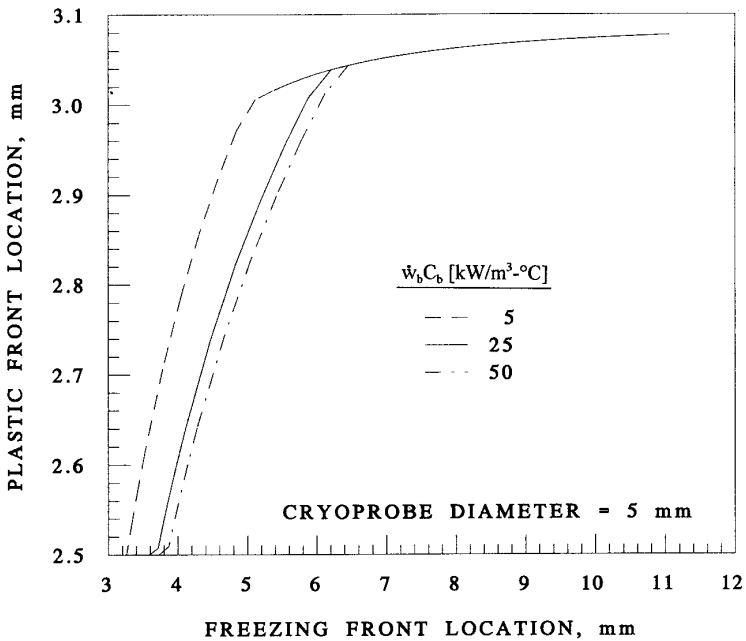


FIG. 3. Plastic front location as a function of freezing front location for the case of relatively high yield strain,  $\epsilon_y = 5 \times 10^{-3}$  (case A).

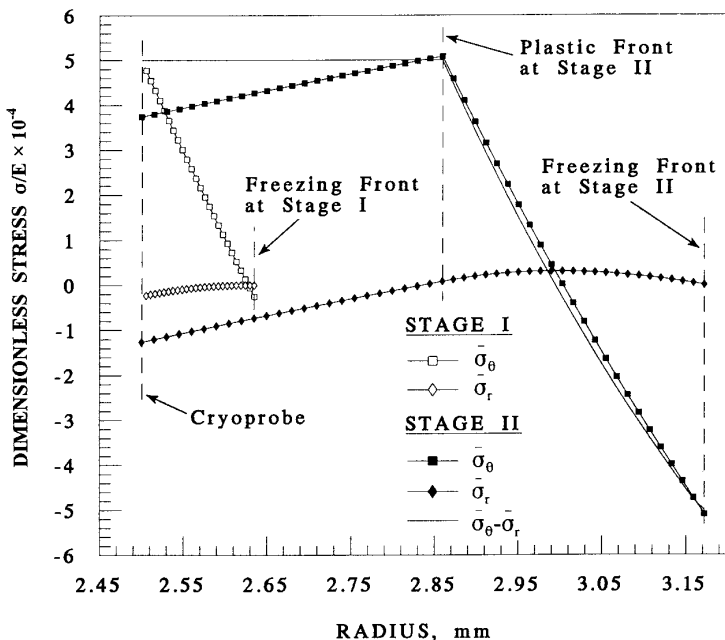


FIG. 4. Stress distributions around a spherical cryoprobe, for the case of normal yield strain,  $\epsilon_y = 5 \times 10^{-4}$  (case B).

as the tangential stress reaches the yield strength at the freezing front. The stress analysis was not performed beyond this point. It can be seen from Fig. 4 that for an expected yield strain the tangential stresses are much higher than the radial stresses. At the cryoprobe surface the tangential stress is always tensile while the radial stress is always compressive. At a certain point in time the assumption of elastic deformation at the freezing front is not valid any more because the tangential stress becomes larger in magnitude than the yield strength (since  $\sigma_r = 0$  at this surface, the yield condition becomes  $|\sigma_\theta| = \sigma_y$ ). After the end of stage II, it can be expected that a new plastic region will be formed near the freezing front and that the elastic region will become narrower with time.

It is emphasized that the temperature gradients near the freezing front in the real freezing process will be more moderate than those in the present solution, as the phase-change process takes place over a temperature range and not at a specific temperature,  $T_m$ . Therefore,

the new plastic region is not actually expected to be formed sharply at single temperature, but over a temperature range. However, the phenomenon observed in case B—the possibility of plastic deformation near the freezing front—is very significant. This observation suggests a linkage between maximal cryodestruction and plastic deformation near the freezing front.

Due to the differences between cases A and B, the relationship between the yield strain and cryoprobe temperature at which yielding occurs at the freezing front is studied next (Fig. 5). The plastic front temperature at this instant is presented in Fig. 5 as well. The above relationship is presented for cryoprobe diameters in the range of 2.5 to 7.5 mm. These results are for a cryoprobe cooling rate of 200°C/min. All curves in Fig. 5 end as the cryoprobe temperature reaches  $-196^\circ\text{C}$  which is the liquid nitrogen boiling temperature. It can be seen from Fig. 5 that the results are relatively insensitive to the cryoprobe diameter in the yield strain range of  $\epsilon_y = 0$  to 1.5

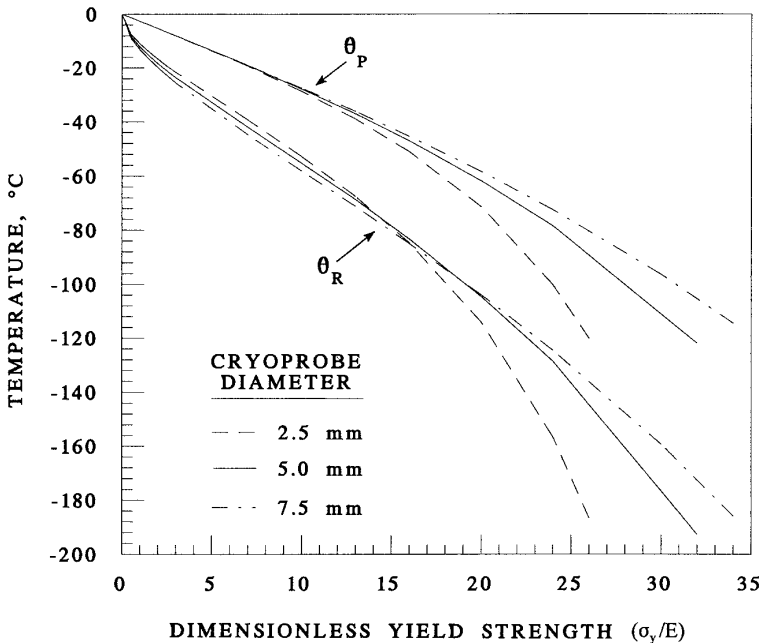


FIG. 5. Cryoprobe temperature and plastic front temperature as plastic deformation starts to develop near the freezing front.

$\times 10^{-3}$ , in which the yield strain is expected to be found. Note also that there is a similarity relation between the cryoprobe temperature and the plastic front temperature as a function of the yield strain. The thermal stress formation transitions from that of case B to that of case A when  $\epsilon_y$  equals  $2.5 \times 10^{-3}$ ,  $3.2 \times 10^{-3}$ , and  $3.4 \times 10^{-3}$  for cryoprobe diameters of 2.5, 5, and 7.5 mm, respectively.

Figure 6 presents the ratio of plastic front location to freezing front location as a function of the yield strain, for the same set of parameters. From Fig. 6 it can be seen that the ratio  $P/S$  is almost a linear function of the yield strain for a specific cryoprobe diameter; it increases with the cryoprobe diameter and decreases as the yield strain. Therefore, it is suggested that larger cryoprobes will cause plastic deformation in a larger portion of the frozen region.

Finally, the relationship between the cooling rate at the cryoprobe and the plastic deformation is studied. Figure 7 presents the cryoprobe temperature at the end of stage II

of case B, when plastic deformation starts to form near the freezing front, as a function of the cryoprobe cooling rate ( $\sigma_y = 5 \times 10^{-4}$ ). Figure 8 presents the ratio of plastic front location to freezing front location as a function of the cryoprobe cooling rate, or the portion of plastic deformation in the frozen region when an additional plastic region starts to form (near the freezing front). Figure 8 presents the dimensionless freezing front location as well, at the end of stage II, as function of the cooling rate. It can be seen from Fig. 7 that as the cooling rate increases the cryoprobe temperature that is required to start plastic deformation near the freezing front decreases. It can be seen from Fig. 8 that the portion of plastic deformation increases with the cooling rate, while the freezing front location at the end of stage II decreases with the cooling rates. Finally, both the freezing front location and the portion of plastic deformation at the end of stage II are insensitive to the cryoprobe diameter for high cooling rates.

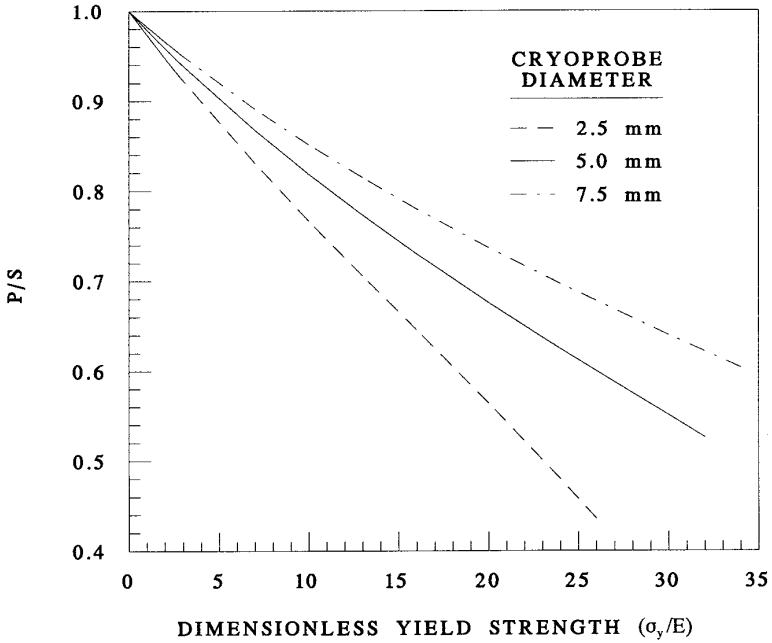


FIG. 6. The ratio of plastic front location to freezing front location,  $P/S$ , as plastic deformation starts to develop near the freezing point.

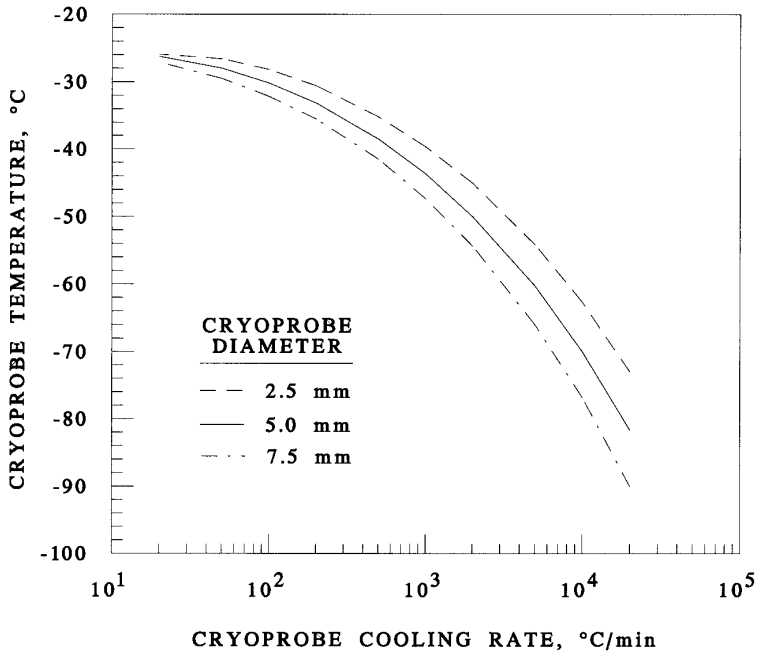


FIG. 7. Cryoprobe temperature as plastic deformation starts to develop near the freezing front.

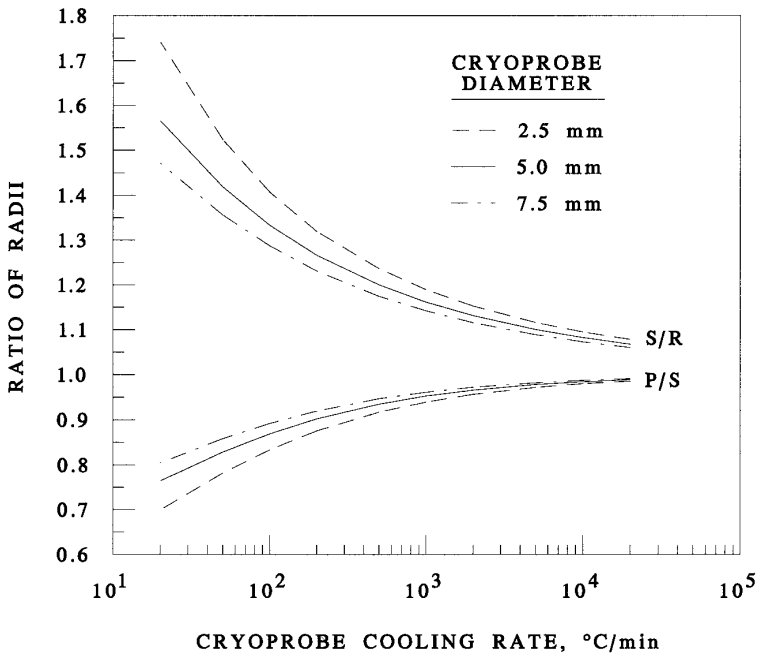


FIG. 8. The ratio of plastic front location to freezing front location,  $P/S$ , and the dimensionless freezing front location,  $S/R$ , as plastic deformation starts to develop near the freezing front.

#### SUMMARY AND CONCLUSIONS

A new mathematical solution for the freezing of biological tissues around a cryosurgical probe has been presented. This solution is an improvement over an earlier solution in that it is suitable for high Stephan numbers and allows for a temperature-dependent forcing function at the cryoprobe. The differences between the earlier and the new solutions were found to be very significant for short times, when the thermal stresses may be as high as the yield strength.

A new solution for the thermal stresses around cryosurgical probe is further presented, using the freezing process temperature solution. The thermal stress solution is based on an elastic-perfectly plastic model for the deformation of frozen biological tissue. The thermal stress problem is separated into two stages: in the first stage the entire frozen region is elastic; in the second stage there is plastic deformation around the cryoprobe.

Assuming typical thermophysical proper-

ties of soft biological tissues for the heat transfer solution, and typical physical properties of ice for the thermal stress solution, it was observed that two distinct behaviors can occur. For high yield strain (case A) plastic and elastic regions will be formed as described above. For normal and low yield strain (case B) an additional plastic region will start to form near the freezing front due to high compressive stresses in the tangential direction. The latter behavior is more likely to prevail under conditions typical of ordinary cryoprocurement.

Assuming that plastic deformation is related to cryodestruction, case B is more severe than case A. A parametric study was performed to identify the best cooling protocol for maximal plastic deformation. From the parametric study it was found that larger cryoprobes will cause higher thermal stresses, that plastic deformation near the freezing front starts earlier for higher cooling rates and larger cryoprobes, and that higher cooling rates lower the cryo-

probe temperature needed for plastic deformation near the freezing front.

$y$  yield  
 $\theta$  tangential direction

## APPENDIX: NOMENCLATURE

$B_i$  integration constant of stress distribution; dimensionless for  $i = 1$  and  $2$ ;  $m^{-1}$  for  $i = 3$ ; and  $m^3$  for  $i = 4$

$C$  volumetric specific heat,  $J/m^3\text{-}^\circ\text{C}$

$D$  cryoprobe diameter,  $m$

$E$  Young's module,  $N/m^2$

$H$  cryoprobe cooling rate,  $^\circ\text{C}/s$

$k$  thermal conductivity,  $W/m\text{-}^\circ\text{C}$

$L$  volumetric latent heat,  $J/m^3$

$P$  plastic front location,  $m$

$r$  radial coordinate,  $m$

$R$  cryoprobe radius,  $m$

$S$  freezing front location,  $m$

$St_i$  Stephan number;  $C_l(T_b - T_m)/L$  for  $i = 1$ , and  $C_f(T_m - T_R)/L$  for  $i = f$

$t$  time,  $s$

$u$  displacement,  $m$

$T$  temperature,  $^\circ\text{C}$

$\dot{w}_b$  blood perfusion,  $ml$  blood/ $ml$  tissue per second

*Greek*

$\alpha$  thermal diffusivity,  $m^2/s$

$\beta$  thermal expansion coefficient,  $liters/^\circ\text{C}$

$\gamma$  temperature distribution parameter, Eq. [15],  $liters/m$

$\epsilon$  strain

$\lambda$  plastic strain

$\nu$  Poisson's ratio

$\sigma$  stress,  $N/m^2$

$\bar{\sigma}$  dimensionless stress,  $\sigma/E$

$\theta$  temperature difference, Eq. [9],  $^\circ\text{C}$

*Indexes*

$0$  initial

$b$  blood

$E$  elastic

$f$  frozen

$l$  unfrozen

$m$  phase change

$P$  plastic

$r$  radial direction

$R$  cryoprobe surface

$T$  thermal

## ACKNOWLEDGMENT

This research was supported in part by Allegheny-Singer Research Institute (95-028-3P), Pittsburgh, PA.

## REFERENCES

- Altman, P. L., and Dittmer, D. S. "Respiration and Circulation," Federation of American Societies for Experimental Biology (Data Handbook), Bethesda, MD, 1971.
- Ashby, M. F., and Jones, D. R. H. "Engineering Materials," Pergamon Press, Elmsford, NY, 1980.
- Boley, B. A., and Weiner, J. H. "Theory of Thermal Stresses," Wiley, New York, 1960.
- Charny, C. K. Mathematical models of bioheat transfer. In "Advances in Heat Transfer" (J. P. Hartnett, T. F. Irvine, and Y. I. Cho, Eds.), pp. 19-156, Academic Press, San Diego, 1992.
- Chato, J. C. Selected thermophysical properties of biological materials, In "Heat Transfer in Biology and Medicine" (A. Shitzer and R. C. Eberhart, Eds.), pp. 413-418, Plenum, New York, 1985.
- Chen, M. M., and Holmes, K. R. Microvascular contributions in tissue heat transfer. *Ann. N.Y. Acad. Sci.* **335**, 137 (1980).
- Cooper, T. E., and Trezek, G. J. Rate of lesion growth around spherical and cylindrical cryoprobe. *Cryobiology* **7**, 183-190 (1971).
- Diller, K. R. Modeling of bioheat transfer processes at high and low temperatures. In "Advances in Heat Transfer" (J. P. Hartnett, T. F. Irvine, and Y. I. Cho, Eds.), pp. 157-358, Academic Press, San Diego, 1992.
- Dykins, J. E. Tensile and flexure properties of saline ice. In "Physics of Ice" (N. Riehl, B. Bullemer, and H. Engelhardt, Eds.), Plenum, New York, 1969.
- Fahy, G. M. Analysis of "solution effect" injury: Cooling rate dependence of the functional and morphological sequelae of freezing in rabbit renal cortex protected with dimethyl sulfoxide. *Cryobiology* **18**, 550-570 (1981).
- Fahy, G. M., Saur, J., and Williams, R. J. Physical problems with the vitrification of large biological systems. *Cryobiology* **27**, 492-510 (1990).
- Fletcher, N. H. "The Chemical Physics of Ice," Cambridge Univ. Press, Cambridge, UK, 1970.
- Gage, A. A. Critical temperature for skin necrosis in experimental cryosurgery. *Cryobiology* **19**, 273-281 (1982).
- Gage, A. A., Guest, K., Montes, M., Garuna, J. A., and Whalen, D. A., Jr. Effect of varying freezing and thawing rates in experimental cryosurgery. *Cryobiology* **22**, 175-182 (1985).

15. Goodman, T. R. The heat balance integral method and its application to problems involving a change of phase. *Trans. ASME*, **80**, 335–342 (1958).
16. Hayes, L. J., and Diller, K. R. A finite elements model for phase-change heat transfer in composite tissue with blood perfusion. *Trans. Instr. Soc. Am.* **22**(4), 33–38 (1983).
17. Hill, R. "The Mathematical Theory of Plasticity," Oxford Univ. Press, London, 1960.
18. Hunt, C. J., Song, Y. C., Bateson, A. J., and Pegg, E. D. Fractures in cryopreserved arteries. *Cryobiology* **31**, 506–515 (1994).
19. Ishiguro, H., and Rubinsky, B. Mechanical interaction between ice crystals and red blood cells during directional solidification. *Cryobiology* **31**, 483–500 (1994).
20. Klinger, H. G. Heat transfer in perfused biological tissue. I. General theory. *Bull. Math. Biol.* **36**, 403 (1974).
21. Lee, C. Y. C., and Rubinsky, B. A multi-dimensional model of momentum and mass transfer in the liver. *Int. J. Heat Mass Transfer* **32**, 2421–2434 (1989).
22. Mazur, P. Kinetics of water loss from cells at subzero temperatures and the likelihood of intracellular freezing. *J. Gen. Phys.* **44**, 347–369 (1963).
23. Mazur, P., Leibo, S., and Chu, E. H. Y. A two-factor hypothesis of freezing injury. *Exp. Cell Res.* **71**, 345–355 (1972).
24. McGrath, J. J. Low temperature injury processes. In "Advances in Bioheat and Mass Transfer," (R. B. Roemer, Ed.), Vol. 268, pp. 125–132, ASME HTD, New Orleans, LA, 1993.
25. Miller, R. H., and Mazur, P. Survival of frozen-thawed human red cells as a function of cooling and warming velocities. *Cryobiology* **13**, 404–414 (1976).
26. Murthy, T. K. S., Connor, J. J., and Brebbia, C. A. "Ice Technology," Proceedings, 1st International Conference, Cambridge, MA, Springer-Verlag, Berlin, 1986.
27. Pennes, H. H. Analysis of tissue and arterial blood temperatures in the resting human forearm. *J. Appl. Physiol.* **1**, 93–122 (1948).
28. Rabin, Y., and Korin, E. An efficient numerical solution for the multidimensional solidification (or melting) problem using a microcomputer. *Int. J. Heat Mass Transfer* **36**(3), 673–683 (1993).
29. Rabin, Y., Coleman, R., Mordohovich, D., Ber, R., and Shitzer, A. A new cryosurgical device for controlled freezing. II. *In vivo* experiments on skeletal muscle of rabbit hindlimbs. *Cryobiology* **33**, 93–105 (1996).
30. Rand, R. W., Rand, R. P., Eggerding, F. A., Field, M., Denbesten, L., King, W., and Camici, S. Cryolumpectomy for breast cancer: an experimental study. *Cryobiology* **22**, 307–318 (1985).
31. Rubinsky, B., Cravalho, E. G., and Mikic, B. Thermal stress in frozen organs. *Cryobiology* **17**, 66–73 (1980).
32. Rubinsky, B., and Cravalho, E. G. A finite-element method for the solution of one-dimensional phase change problem. *Int. J. Heat Mass Transfer* **24**, 1587–1589 (1981).
33. Smith, J. J., and Fraser, J. An estimation of tissue damage and thermal history in cryolesion. *Cryobiology* **11**, 139–147 (1974).
34. Weeks, W., and Assur, A. "The Mechanical Properties of Sea Ice," Cold Regions Research & Engineering Laboratory, U.S. Army, Hanover, NH, 1967.
35. Weinbaum, S., and Jiji, L. M. A new simplified bio-heat equation for the effect of blood flow on local average tissue temperature. *ASME J. Biomech. Eng.* **107**, 131–136 (1985).
36. Wulff, W. The energy conservation equation for living tissues. *IEEE Trans. Biomed. Eng.* **BME-21**, 494 (1974).